Modern Physics Letters B, Vol. 24, No. 13 (2010) 1287–1290

DOI: 10.1142/S021798491002344X

World Scientific
www.worldscientific.com

LARGE-EDDY SIMULATION OF OPPOSING-JET-PERTURBED SUPERSONIC FLOWS PAST A HEMISPHERICAL NOSE

LI-WEI CHEN, CHANG-YUE XU and XI-YUN LU*

Department of Modern Mechanics, University of Science and Technology of China, Hefei, Anhui 230026, China
**xlu@ustc.edu.cn*

Received 1 June 2009

A supersonic flow past a hemispherical nose with an opposing jet placed on its axis has been investigated using large eddy simulation. We find that the flow behaviors depend mainly on the jet total pressure ratio and can be classified into three typical flow regimes of unstable, stable and transition. The unstable flow regime is characterized by an oscillatory bow shock with a multi-jet-cell structure and the stable flow regime by a steady bow shock with a single jet cell. The transition regime lies between the unstable and stable ones with a complex flow evolution. Turbulence statistics are further analyzed to reveal the relevant turbulent behaviors in the three flow regimes. The results obtained in this study provide a physical insight into the understanding of the mechanisms underlying this complex flow.

Keywords: Large-eddy simulation; opposing jet; shock wave; turbulent flow.

1. Introduction

The flow phenomena associated with an opposing-jet-perturbed supersonic flow past a bluff body are of importance in both fundamentals and applications. The early experiments mainly investigated the mean flow characteristics and revealed that the jet total pressure ratio is a key parameter governing the complex flow evolution.[1,2] Then, Debiève *et al.* provided the measurement of turbulence statistics and noticed that turbulent boundary layer is significantly influenced by external flow and vortical structures.[3] Although some numerical simulations using the Reynolds-averaged Navier-Stokes equations[4] or laminar model[5] have been performed, the relevant physical flow behaviors are still unclear and are deserved to be studied.

In the present study, a supersonic flow past a hemispherical nose with an opposing jet placed on its axis is investigated for several jet total pressure ratios. Large eddy simulation is implemented in solving the Favre-filtered compressible Navier–Stokes equations.[6] The motivation of this work is to study various fundamental mechanisms dictating the complex flow phenomena.

2. Mathematical Formulation and Numerical Methods

The Favre-filtered compressible Navier-Stokes equations are numerically solved by the finite-volume method.[6] Large eddy simulation is implemented with dynamic subgrid scale models.[6] The convective terms are discretized by a modified second-order central/upwind hybrid scheme, and the viscous terms by a second-order central difference. Time advancement is performed by an implicit approximate-factorization method with sub-iterations to ensure a second-order accuracy.

The initial condition is set as the incoming flow quantities. The far field boundary conditions are treated by local one-dimensional Riemann invariants. No-slip and adiabatic conditions are applied on the surface. The inflow boundary condition is explicitly treated using a specified velocity and uniform static pressure profile.[7] The density profile is obtained using the Crocco-Busemann relation.

3. Results and Discussion

We consider a supersonic flow at $M_\infty = 2.5$ past a hemispherical nose perturbed by an opposing sonic jet on its axis. The jet total temperature ratio $\mathcal{T} = T_{0j}/T_{0\infty}$ is 1.0 with $T_{0\infty} = 294K$. The jet total pressure ratios $\mathcal{P} = p_{0j}/p_{0\infty}$ are chosen as 0.816, 1.0, and 1.633 according to the experiment.[5] The Reynolds number based on the sphere diameter D is 1.47×10^6. The jet diameter is $0.1D$. To clearly present the postprocess, some symbols are introduced as follows. $\langle\ \rangle$ means the average in time and in the azimuthal direction, and $\{f\} = \langle\bar{\rho}f\rangle/\langle\bar{\rho}\rangle$ with a variable f. Then, the fluctuations are obtained as $p' = \bar{p} - \langle\bar{p}\rangle$, and $u_i'' = \tilde{u}_i - \{\tilde{u}_i\}$. $\langle p'^2\rangle^{1/2}$ and $\{u_i''^2\}^{1/2}$ are noted as p'_{rms} and σ_{u_i}, respectively.

To visualize the instantaneous flow structures, the iso-contours of $\|\nabla\bar{\rho}\|$ in the cross-section are shown in Fig. 1. The jet appears to be regular reflection type[5] and multi-cell structure shown in Fig. 1(a) for $\mathcal{P} = 0.816$. The bow shock exhibits unsteady behavior with a low frequency movement. The reattached shock is formed by the coalesced waves. The evolution of the jet back to the nose results in a complicated conical shear layer and a toroidal recirculation zone. This flow behavior is classified as the unstable flow regime.[2] As shown in Fig. 1(b) for $\mathcal{P} = 1.633$, the bow shock stand-off distance decreases and the unsteadiness becomes weak. A single jet cell forms with a well established Mach disk and barrel shock. This flow is classified as the stable flow regime.[2] The transition flow regime at $\mathcal{P} = 1.0$ mostly appears like the unstable flow evolution but has an intermittent behavior similar to the flow pattern in the stable flow regime. As a regular reflection changes to a Mach reflection, an abrupt change of the shock structure in the first cell occurs. When the jet flow across the Mach disk becomes subsonic, the shock system shrinks and the second cell disappears as shown in Fig. 1(c). Then, the jet gradually increases its length so that the bow shock moves away from the nose as depicted in Fig. 1(d). Finally, the jet is terminated by a normal shock in the second cell like the unstable flow behavior again.

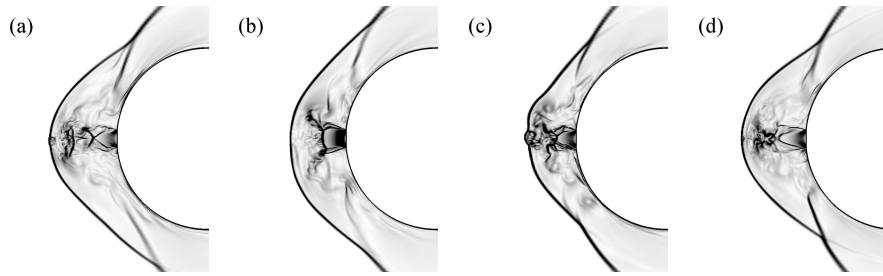

Fig. 1. Instantaneous flow fields visualized by iso-contours of $\|\nabla\bar{\rho}\|$ in the cross-section: (a) $\mathcal{P} = 0.816$, (b) $\mathcal{P} = 1.633$, (c) and (d) $\mathcal{P} = 1.0$.

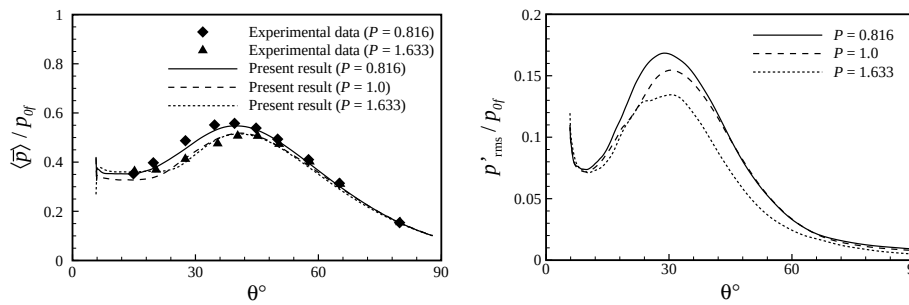

Fig. 2. Distributions of (a) mean pressure with the experimental data and (b) pressure fluctuation on the surface.

The mean wall pressure distributions $\langle\bar{p}\rangle/p_{0f}$ are shown in Fig. 2(a) for comparison with the experimental data,[5] where p_{0f} is the stagnation pressure. The present results agree well with the experiment.[5] The low-pressure plateau region corresponds to the toroidal recirculation zone. The pressure reaches a maximum p_{max} at $\theta = 37°$ approximately. Figure 2(b) shows the normalized pressure fluctuations along the surface. The fluctuations increase after the minimum at $\theta = 10°$, associated with the organized shear layer structures which become stronger and move closer to the surface.[8] The fluctuations reach a maximum of 0.17 for the unstable flow regime and 0.13 for the stable flow regime at around $\theta = 31°$ and then decrease along the surface, related to the acceleration and convex streamline curvature.[3]

The turbulence field is mainly influenced by the conical shear layer due to the deviation of the jet. The streamwise evolution of the positive peak shear stress $\{u_x''u_r''\}_{max}/U_\infty^2$ in the shear layer is shown in Fig. 3(a). The profiles in the unstable and transition flow regime appear higher due to the global unsteadiness. Along the shear layer, the first maximum is related to the formation of vortex-ring-like coherent structures after the jet reverse its direction.[9] The shear stress decreases as the coherent structures are distorted and convected downstream, and then increases rapidly to reach the second maximum related to the onset of the recompression. The

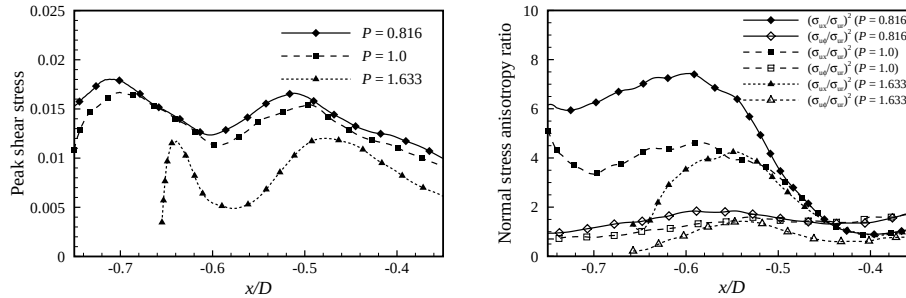

Fig. 3. Streamwise evolution of (a) peak shear stress and (b) normal stress anisotropy ratio along the conical shear layer.

shear stress decreases monotonically after $x/D = -0.5$ due to the convex streamline curvature near the surface.

The streamwise development of the Reynolds stress anisotropy is shown in Fig. 3(b) by a primary-to-secondary stress ratio $(\sigma_{ux}/\sigma_{ur})^2$ and a secondary-to-secondary stress ratio $(\sigma_{u\phi}/\sigma_{ur})^2$, measured at the peak shear stress location in the conical shear layer. Before the onset of the recompression, the $(\sigma_{ux}/\sigma_{ur})^2$ is around 7.5 in the unstable flow regime and 4.0 in the other flow regimes, indicating that the streamwise normal stress is dominant especially in the unstable flow regime. The ratios quickly decay to 1.0 approximately after $x/D = -0.5$, denoting that the streamwise fluctuations are damped to the same order as the radial ones due to the reattachment. The $(\sigma_{u\phi}/\sigma_{ur})^2$ maintains around 1.0, indicating little difference in the turbulence energy redistribution mechanism among these components.[10]

Acknowledgment

This work was supported by the National Natural Science Foundation of China (Nos. 90405007 and 10832010), the Innovative Foundation of the Chinese Academy of Sciences (No. KJCX2-YW-L05), and the 111 Project (No. B07033).

References

1. P. J. Finley, *J. Fluid Mech.* **26** (1966) 337.
2. K. Karashima and K. Sato, *Bull. ISAS* **11** (1975) 53.
3. J. F. Debiève, J. P. Ardissone and J. P. Dussauge, *J. Turb.* **4** (2003) 1.
4. J. S. Shang, J. Hayes, K. Wurtzler and W. Strang, *AIAA J.* **39** (2001) 1159.
5. M. Fujita, *AIAA J.* **33** (1995) 1850.
6. X.-Y. Lu, S. W. Wang, H. G. Sung, S. Y. Hsieh and V. Yang, *J. Fluid Mech.* **527** (2005) 171.
7. D. J. Bodony and S. K. Lele, *Phys. Fluids* **17** (2005) 085103.
8. L. M. Hudy, A. M. Naguib and W. M. Humphreys, *Phys. Fluids* **15** (2003) 706.
9. M. Yoda and H. E. Fiedler, *Exp. Fluids* **21** (1996) 427.
10. J. L. Herrin and J. C. Dutton, *Phys. Fluids* **9** (1997) 3502.